# Chapter 1
# Contact Angle and Wetting Properties

**Yuehua Yuan and T. Randall Lee**

**Abstract** This chapter highlights a variety of techniques that are commonly used to measure contact angles, including the conventional telescope-goniometer method, the Wilhelmy balance method, and the more recently developed drop-shape analysis methods. The various applications and limitations of these techniques are described. Notably, studies of ultrasmall droplets on solid surfaces allow wetting theories to be tested down to the nanometer scale, bringing new insight to contact angle phenomena and wetting behavior.

## 1.1 Introduction

The topic of wetting has received tremendous interest from both fundamental and applied points of view. It plays an important role in many industrial processes, such as oil recovery, lubrication, liquid coating, printing, and spray quenching [1–6]. In recent years, there has been an increasing interest in the study of superhydrophobic surfaces, due to their potential applications in, for example, self-cleaning, nanofluidics, and electrowetting [7–12]. Wettability studies usually involve the measurement of contact angles as the primary data, which indicates the degree of wetting when a solid and liquid interact. Small contact angles ($\ll 90°$) correspond to high wettability, while large contact angles ($\gg 90°$) correspond to low wettability.

This chapter will begin with an introduction of the fundamental science behind wetting and contact angle phenomena, followed by a comprehensive description of the various techniques used to measure contact angles, as well as their applications and limitations in terms of the geometric forms of solid samples. Most of the techniques can be classified into two main groups: the direct optical method and the indirect force method. Calculations based on measured contact angle values yield an important parameter—the solid surface tension, which quantifies the

Y. Yuan · T.R. Lee (✉)
Department of Chemistry, University of Houston, 4800 Calhoun Road, Houston, TX 77204-5003, USA
e-mail: trlee@uh.edu

Y. Yuan
e-mail: yyuan2@uh.edu

G. Bracco, B. Holst (eds.), *Surface Science Techniques*,
Springer Series in Surface Sciences 51, DOI 10.1007/978-3-642-34243-1_1,

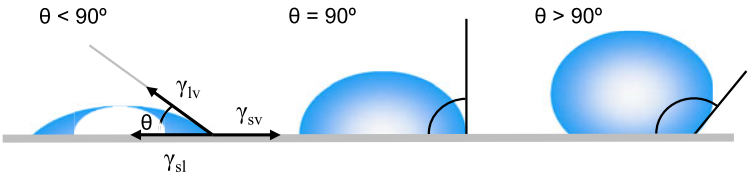


**Fig. 1.1** Illustration of contact angles formed by sessile liquid drops on a smooth homogeneous solid surface

wetting characteristics of a solid material. The criteria of calculating solid surface tension based on experimental contact angle values will be discussed. Finally, the most up-to-date contact angle measurement techniques will be presented and discussed.

## 1.2 Theoretical Background

### *1.2.1 Surface Tension and Contact Angle—Young's Equation*

Consider a liquid drop resting on a flat, horizontal solid surface (Fig. 1.1). The contact angle is defined as the angle formed by the intersection of the liquid-solid interface and the liquid-vapor interface (geometrically acquired by applying a tangent line from the contact point along the liquid-vapor interface in the droplet profile). The interface where solid, liquid, and vapor co-exist is referred to as the "three-phase contact line". Figure 1.1 shows that a small contact angle is observed when the liquid spreads on the surface, while a large contact angle is observed when the liquid beads on the surface. More specifically, a contact angle less than 90° indicates that wetting of the surface is favorable, and the fluid will spread over a large area on the surface; while contact angles greater than 90° generally means that wetting of the surface is unfavorable so the fluid will minimize its contact with the surface and form a compact liquid droplet. For example, complete wetting occurs when the contact angle is 0°, as the droplet turns into a flat puddle. For superhydrophobic surfaces, water contact angles are usually greater than 150°, showing almost no contact between the liquid drop and the surface, which can rationalize the "lotus effect" [13]. Furthermore, contact angles are not limited to the liquid-vapor interface on a solid; they are also applicable to the liquid-liquid interface on a solid.

Ideally, the shape of a liquid droplet is determined by the surface tension of the liquid. In a pure liquid, each molecule in the bulk is pulled equally in every direction by neighboring liquid molecules, resulting in a net force of zero. However, the molecules exposed at the surface do not have neighboring molecules in all directions to provide a balanced net force. Instead, they are pulled inward by the neighboring molecules (Fig. 1.2), creating an internal pressure. As a result, the liquid voluntarily contracts its surface area to maintain the lowest surface free

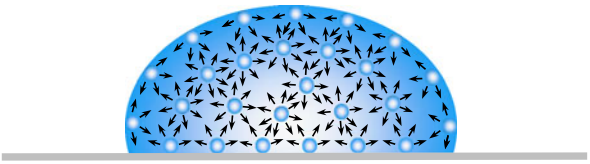

**Fig. 1.2** Surface tension is caused by the unbalanced forces of liquid molecules at the surface

energy. From everyday life, we know that small droplets and bubbles are spherical, which gives the minimum surface area for a fixed volume. This intermolecular force to contract the surface is called the surface tension, and it is responsible for the shape of liquid droplets. In practice, external forces such as gravity deform the droplet; consequently, the contact angle is determined by a combination of surface tension and external forces (usually gravity). Theoretically, the contact angle is expected to be characteristic for a given solid-liquid system in a specific environment [14].

As first described by Thomas Young [15] in 1805, the contact angle of a liquid drop on an ideal solid surface is defined by the mechanical equilibrium of the drop under the action of three interfacial tensions (Fig. 1.1):

$$\gamma_{lv} \cos\theta_Y = \gamma_{sv} - \gamma_{sl} \tag{1.1}$$

where $\gamma_{lv}$, $\gamma_{sv}$, and $\gamma_{sl}$ represent the liquid-vapor, solid-vapor, and solid-liquid interfacial tensions, respectively, and $\theta_Y$ is the contact angle. (1.1) is usually referred to as Young's equation, and $\theta_Y$ is Young's contact angle.

### *1.2.2 Contact Angle Hysteresis*

From Young's equation applied to a specific liquid-solid system, three thermodynamic parameters $\gamma_{lv}$, $\gamma_{sv}$, and $\gamma_{sl}$ determine a single and unique contact angle $\theta_Y$. In practice, however, there exist many metastable states of a droplet on a solid, and the observed contact angles are usually not equal to $\theta_Y$. The phenomenon of wetting is more than just a static state. The liquid moves to expose its fresh surface and to wet the fresh surface of the solid in turn. The measurement of a single static contact angle to characterize wetting behavior is no longer adequate. If the three-phase contact line is in actual motion, the contact angle produced is called a "dynamic" contact angle. In particular, the contact angles formed by expanding and contracting the liquid are referred to as the advancing contact angle $\theta_a$ and the receding contact angle $\theta_r$, respectively (Fig. 1.3). These angles fall within a range, with the advancing angles approaching a maximum value, and the receding angles approaching a minimum value. Dynamic contact angles can be measured at various rates of speed. At a low speed, it should be close or equal to a properly measured static contact angle. The difference between the advancing angle and the receding angle is called the hysteresis ($H$):

$$H = \theta_a - \theta_r \tag{1.2}$$

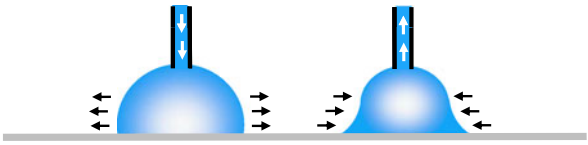

**Fig. 1.3** Illustration of advancing and receding contact angles

The significance of contact angle hysteresis has been extensively investigated [16–20], and the general conclusion is that it arises from surface roughness and/or heterogeneity. For surfaces that are not homogeneous, there exist domains that present barriers to the motion of the contact line. For example, hydrophobic domains will pin the motion of the water front as it advances, causing an increase in the observed contact angle; the same domains will hold back the contracting motion of the water front when the water recedes, thus leading to a decrease in the observed contact angle. In cases that surface roughness plays the role of generating hysteresis, the actual microscopic variations of slope on the surface create barriers that pin the motion of the contact line and alter the macroscopic contact angles. Interpreting such contact angle data in terms of Young's equation can be misleading because the equation fails to consider surface topography.

Due to the complexity of contact angle phenomena, the experimentally observed contact angle might or might not be equal to Young's contact angle $\theta_Y$ [21, 22]. However, on ideal solid surfaces, there is no contact angle hysteresis, and the experimentally observed contact angle is Young's contact angle $\theta_Y$. On smooth but chemically heterogeneous solid surfaces, the experimentally observed contact angle might not be equal to $\theta_Y$. Nevertheless, the experimental advancing contact angle $\theta_a$ might be expected to be a good approximation of $\theta_Y$ [21, 22], while the experimental receding angle $\theta_r$ is usually found to have less reproducibility due to liquid sorption or solid swelling [23]. On rough solid surfaces, there is usually no correlation between $\theta_a$ and $\theta_Y$. All contact angles on rough surfaces are largely meaningless in terms of Young's equation [21, 22]. The thermodynamic equilibrium contact angles on rough and heterogeneous surfaces are called Wenzel [24] and Cassie-Baxter angles [25], respectively. They are not equivalent to Young's contact angle.

There are as yet no general guidelines regarding how smooth a solid surface must be for surface roughness not to have an obvious impact on the contact angle. It is therefore recommended that the solid surface should be prepared as smooth as possible, and as inert to the liquids of interest as possible. Several techniques for the preparation of smooth homogeneous solid surfaces have been developed; these include: heat pressing [26], solvent casting [27, 28], self-assembled monolayers [29, 30], dip coating [31, 32], vapor deposition [33, 34], and surface polishing [35, 36].

**Fig. 1.4** A ramé-hart contact angle telescope-goniometer

## 1.3 Experimental Setup and Method

### *1.3.1 Direct Measurement by Telescope-Goniometer*

The most widely used technique of contact angle measurement is a direct measurement of the tangent angle at the three-phase contact point on a sessile drop profile. Bigelow et al. [37] set up a simple and convenient instrument, which they referred to as a "telescope-goniometer" to measure contact angles of various liquids on polished surfaces. Later, the first commercial contact angle goniometer, designed by W.A. Zisman, was manufactured by ramé-hart instrument company in the early 1960s (Fig. 1.4).

The equipment consists of a horizontal stage to mount a solid or liquid sample, a micrometer pipette to form a liquid drop, an illumination source, and a telescope equipped with a protractor eyepiece. The measurement was achieved by simply aligning the tangent of the sessile drop profile at the contact point with the surface and reading the protractor through the eyepiece. Over the years, modifications of the equipment have been made to improve the accuracy and precision. A camera can be integrated to take photographs of the drop profile so as to measure the contact angle at leisure [38]. The use of relatively high magnifications enables a detailed examination of the intersection profile [39]. A motor-driven syringe can be used to control the rate of liquid addition and removal to study advancing, receding, or dynamic contact angles [40].

This direct optical method is advantageous because of its simplicity and the fact that only small amounts of liquid (a few microliters) and small surface substrates (a few square millimeters) are required. On the other hand, there is a relatively higher risk/impact of impurities due to the small size of the liquid and substrate. As for accuracy and reproducibility, the measurement relies on the consistency of the operator in the assignment of the tangent line, which can lead to significant error and inconsistency between multiple users. It is necessary to establish general guidelines for operators to follow. It is suggested that the telescope be tilted down slightly (1 to 2°) off the horizon so that the near edge of the sample stage (out of

focus) is out of the line of sight, and a portion of the profile reflected by the substrate surface is brought into focus, which prevents forming a fuzzy liquid-substrate contact line in the profile. A background light is always used to assist observation, while a specific light source is selected to avoid undesired heating of the liquid or substrate.

To establish an advancing contact angle, it is best to slowly grow the sessile drop to a diameter of approximately 5 mm using a micrometer syringe with a narrow-gauge stainless steel or Teflon needle. The needle must remain in the liquid drop during measurement to avoid undesired vibration. The needle diameter should be as small as possible so it does not distort the drop profile shape. Because, the drop might be unsymmetrical, it is advisable that contact angles be measured on both sides of the liquid drop profile, and to use the averaged result. For a relatively large substrate, contact angles should be measured at multiple points to give an average value that is representative of the entire surface.

The direct goniometer method suffers from another serious limitation because small contact angles (below 20°) cannot be accurately measured due to the uncertainty of assigning a tangent line when the droplet profile is almost flat. Also, the imaging device only focuses on the largest meridian section of the sessile drop, which means the profile image reflects only the contact angle at the point in which the meridian plane intersects the three-phase line. In addition,the dependence of the contact angle on the drop size causes a systematic problem [41, 42]. Surface heterogeneity or roughness could well cause variations of the contact point along the three-phase contact line. Despite all of these issues, the goniometer method is considered to be the most convenient method if high accuracy is not required [43]. It is generally recognized that the direct measurement of sessile drop contact angles with a telescope-goniometer can yield an accuracy of approximately ±2° [43, 44].

Ideally, contact angle measurements should be made inside an enclosed chamber to exclude airborne contamination and establish an equilibrium vapor pressure of the liquid tested, which is especially preferable when the test liquid is volatile. It has been observed that evaporation can cause the liquid front to retract, and that a retreating or an intermediate contact angle is recorded unintentionally. However, the inherent inaccuracy of the direct measurement technique and the use of liquids with high boiling points make the enclosed chamber unnecessary in many cases.

The measurement of the contact angle hysteresis has been recommended as a means to assess the quality of the substrate surface. A “tilted plate” method (also referred to as the “inclined plate” method) was introduced by McDougall and Ockrent [45] (this is not to be confused with the “tilting plate” method in Sect. 1.3.3), who modified the sessile drop method and obtained both advancing and receding contact angles by tilting the solid surface until the drop just begins to move. The contact angles obtained at the lowest point $\theta_{max}$ and the highest point $\theta_{min}$ are considered as the advancing and receding contact angles, respectively (Fig. 1.5). This method was used by Extrand and Kumagai [46, 47] to study the contact angle hysteresis of liquids on a variety of polymer surfaces, including silicon wafers and elastomeric

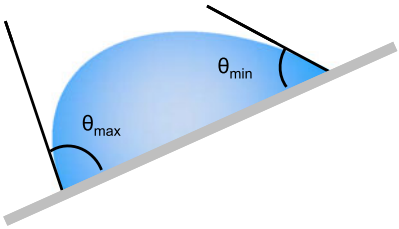


**Fig. 1.5** Illustration of the "tilted plate" method, where $\theta_{max}$ and $\theta_{min}$ are assumed to be $\theta_a$ and $\theta_r$, respectively when the drop just starts to move

surfaces. However, this particular association between the advancing/receding angles and the maximum/minimum contact angles must be used with caution because sometimes they can be quite different [48, 49].

In the early history of contact angle measurement, a platinum wire was used by Zisman and his co-workers [50] to form sessile liquid drops on solid surfaces. A fine platinum wire (about 8 cm long and 0.05–0.10 mm in diameter) was first cleaned by heating to red in a Bunsen burner, then dipped into the liquid and gently flicked to form a pendant drop hanging from the tip of the wire. The drop was then slowly brought into contact with the solid surface, and it flowed off the wire, forming a sessile drop. Although a reproducibility of $\pm 2°$ was claimed [26], there are concerns about the kinetic energy associated with the flowing droplet and the deformation that occurs when removing the platinum wire, which might lead to metastable contact angles.

Phillips and Riddiford [51], as well as McIntyre [52] have analyzed sessile drop profile photographs with a "tangentometer", which consists a mirror mounted at the baseline of the droplet. The mirror is positioned normal to the photograph at the drop tip, and is rotated until the curve of the drop shape forms a smooth, continuous curve with its reflection image in the mirror. Thus, the straight edge becomes the tangent line, and contact angle value is indicated by the protractor that is attached to the mirror. However, this technique still suffers inaccuracy due to the inherent subjectivity of tangentometers [53]. Fisher [54] has acquired a series of contact angle data less than 30° by applying the mass of the drop and the radius of the contact area into a semi-empirical formula that calculates the contact angle value. Langmuir and Schaeffer [55] used the specular reflection from a drop surface to measure the contact angle. Here, a light source above the three-phase contact line is rotated around the sessile drop, until to the height that small changes make the reflected light from the drop disappear or appear abruptly. The degree of rotation indicates the contact angle. This method was later refined by Fort and Patterson [56, 57] and has been used with both sessile drops and menisci on flat plates or inside tubes, with an accuracy of $\pm 1°$.

In the preceding sections, we have focused on techniques that involve measuring a sessile liquid drop on flat solid surfaces, which is the most common system for contact angle measurements. The following sections describe other systems and methods, including measurements of contact angles on solid samples that have different geometric forms (e.g., plates, fibers, and powders).

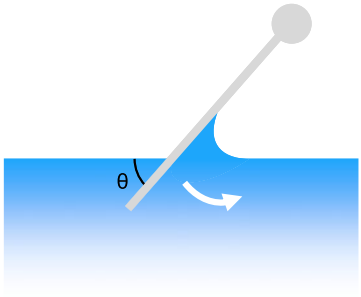


**Fig. 1.6** Illustration of the tilting plate method

### *1.3.2 Captive Bubble Method*

Instead of forming a liquid sessile drop above the solid sample, an air bubble can be formed beneath the solid sample, which is immersed in the testing liquid. The contact angle formed by the air bubble in liquid can also be directly measured. The technique was introduced by Taggart et al. [58], and is now widely referred to as the "captive bubble method". Typically, a small amount of air (about 0.05 ml) is injected into the liquid of interest to form an air bubble underneath the solid surface. Similar to the sessile drop method, the needle should remain in the bubble so as not to disturb the balance of the advancing angle and also to keep the bubble from drifting over the solid surface in case the plate is not perfectly horizontal. The captive bubble method has the advantage of ensuring that the surface is in contact with a saturated atmosphere. It also minimizes the contamination of the solid-vapor interface from sources such as airborne oil droplets. Furthermore, it is much easier to monitor the temperature of the liquid in the captive bubble method than with sessile drops, which makes it possible to study the temperature-dependence of contact angles. On clean smooth polymeric surfaces, good agreement has been observed between sessile drop and captive bubble contact angles [59]. However, due to the nature of the method, the captive bubble method requires far more liquid than the sessile drop method. It can also be problematic when the solid swells after immersion into the liquid, or a film on the solid is dissolved by the liquid.

### *1.3.3 Tilting Plate Method*

The tilting plate method developed by Adam and Jessop [60] was once favored due to its simplicity and relatively lesser dependence on the operator's subjectivity. In this method, a solid plate with one end gripped above the liquid is rotated toward the liquid surface until the end of the plate is immersed in the liquid, forming a meniscus on both sides of the plate. The plate is then tilted slowly until the meniscus becomes horizontal on one side of the plate (Fig. 1.6). The angle between the plate and the horizontal is then the contact angle of interest. An error of $\pm 5^\circ$ was reported, which was attributed to liquid contamination. The disturbance of the liquid by the

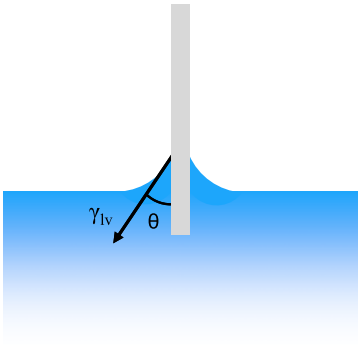


**Fig. 1.7** Illustration of the Wilhelmy balance method

rotating solid plate and the requirement of considerable skills remain the major difficulties in the measurement. Fowkes and Harkins [61] improved the accuracy of the method by using glass barriers to clean the surface and a film balance to detect the presence of impurities on the liquid surface. They also used a microscope with an eyepiece to ensure the edge of the solid-liquid intersection lay on the axis of rotation. This method has also been used to measure small contact angles (less than 10°) [62]. Smedley and Coles [63] employed a scanning laser beam with the tilting plate technique to study the moving contact line, with the intention of making accurate measurements of the contact angle. The technique demonstrates high accuracy and potential to determine the velocity-dependence of dynamic contact angles automatically. Bezuglyi et al. [64] substantially enhanced the precision and reproducibility of the tilting plate technique by applying a high sensitivity thermocapillary (TC) response to the static curvature of the liquid meniscus.

### *1.3.4 Wilhelmy Balance Method*

The Wilhelmy balance method [65] is a widely used technique that indirectly measures contact angle on a solid sample. When a thin, smooth, vertical plate is brought in contact with a liquid, the change in its weight is detected by a balance. The detected force change on the balance is a combination of buoyancy and the force of wetting (the force of gravity remains the same). The wetting force $f$ is defined as (Fig. 1.7):

$$f = \gamma_{lv} p \cos\theta \tag{1.3}$$

where $\gamma_{lv}$ is the liquid surface tension, $p$ is the perimeter of contact line (i.e., the same as the perimeter of solid sample's cross-section) and $\theta$ is the contact angle. Consequently, the total detected force change $F$ on the balance is:

$$F = \gamma_{lv} p \cos\theta - V \Delta\rho g \tag{1.4}$$

where $V$ is the volume of the displaced liquid, $\Delta\rho$ is the difference in density between the liquid and air (or a second liquid), and $g$ is the acceleration of gravity.

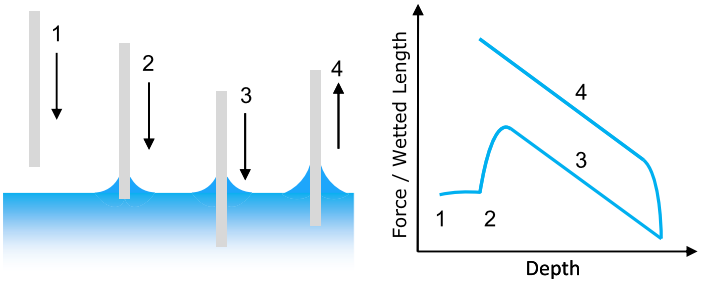


**Fig. 1.8** A submersion cycle for the Wilhelmy balance measurement: (*1*) The sample approaches the liquid, and the force/length is zero. (*2*) The sample is in contact with the liquid surface, forming a contact angle $\theta < 90°$; the liquid rises up, causing a positive wetting force. (*3*) The sample is immersed further, and the increase of buoyancy causes a decrease in the force detected on the balance; the force is measured for the advancing angle. (*4*) The sample is pulled out of the liquid after having reached the desired depth; the force is measured for the receding angle

Thus, as long as the liquid surface tension and the solid perimeter are known, the contact angle value can be readily calculated. In rare cases, when the contact angle is zero and the perimeter is known, the measured force is related directly to the liquid surface tension. A technique developed by Princen [66] enables obtaining a zero contact angle in order to measure liquid surface tension by Wilhelmy balance method.

As the solid sample is pushed into or pulled out of the liquid, an advancing or receding contact angle can be established, respectively. The entire process will appear as illustrated in Fig. 1.8. The Wilhelmy balance technique is an indirect force method. It has several advantages over conventional optical methods. First, the task of measuring an angle is reduced to the measurements of weight and length, which can be performed with high accuracy and without subjectivity. Second, the measured force at any given depth of immersion is already an averaged value. Although this feature does not help determine the heterogeneity, it does automatically give a more accurate contact angle value that reflects the property of the entire sample. In addition, the graph produced by this technique (Fig. 1.8) is useful for studying dynamic contact angles and contact angle hysteresis at different wetting speeds. The smoothness of the curve indicates the heterogeneity of the solid sample. It is even possible to study absorption or surface reorientation by repeating the submersion circle. However, the method also suffers from several drawbacks. The solid sample must be produced with a uniform cross section in the submersion direction. Rods, plates, and fibers with known perimeters are ideal samples, but it is sometimes difficult to measure the perimeter and the wetted length precisely. Other than regular geometries, the sample must have the same composition and topography at all sides, which might be difficult to meet, particularly if one wants to investigate films or anisotropic systems. Also, a sufficient quantity of liquid must be used, which might cause the solid sample to swell and/or absorb vapor unintentionally.

### 1.3.5 Capillary Rise at a Vertical Plate

When a liquid comes in contact with a vertical and infinitely wide plate, it will rise due to the capillary effect. The height of capillary rise $h$ can be determined by the integration of the Laplace equation [67]:

$$\sin\theta = 1 - \frac{\Delta\rho g h^2}{2\gamma_{lv}} \tag{1.5}$$

where $\Delta\rho$ is the difference in density between liquid and vapor, $g$ is the acceleration due to gravity, and $\gamma_{lv}$ is the liquid surface tension. Plates that are about 2 cm wide satisfy the theoretical requirement of being "infinitely" wide. The Wilhelmy balance method can be modified to measure the capillary rise $h$, in order to determine the contact angle $\theta$ [68, 69]. Dynamic contact angles are achieved by moving the plate up or down. This method has been widely used, and has proved to be particularly suitable for measuring the temperature-dependence of contact angles [70]. The method has been automated by Budziak and Neumann [71], and Kwok et al. [72]. For a specially prepared surface that forms a straight meniscus line, an accuracy of $\pm 0.1^\circ$ can be obtained. This technique also inherited most of the advantages and disadvantages of Wilhelmy balance method. In addition, (1.4) and (1.5) can be combined through the relation $\sin^2\theta + \cos^2\theta = 1$, making it possible to determine both contact angle and liquid surface tension at the same time [73–75].

### 1.3.6 Individual Fiber

The direct measurement of contact angles on fibers has been attempted by Schwartz and co-workers [76, 77]. They suspended an individual fiber horizontally in the field of a microscope, and used a goniometer eyepiece to measure the contact angles of drops deposited on the fiber. Rotating the fiber along its longitudinal axis yielded approximate advancing and receding contact angles accordingly. Bascom and Romans [78] improved this method by placing a small platinum ring to hold the liquid drop, and passed a glass filament vertically through the center of the drop. Both advancing and receding contact angles were measured with a microscope as the filament was pulled through the stationary drop. Roe [79] has computed the equilibrium shapes of drops resting on fibers having different diameters. It was shown that the apparent contact angle can become misleading if the drop diameter is much larger than that of the fiber. Due to the small dimensions, large uncertainties exist because the drop curvature and the weight of the drop distort the profile where the fiber and liquid intersect. The equilibrium meniscus near a floating fiber on a liquid can also be used to calculate the contact angle [80–82]. The reflection method developed by Fort and Patterson has also been used to measure contact angles on fibers [56]. However, in practice, the relatively small depth of immersion can make it difficult to obtain good accuracy.

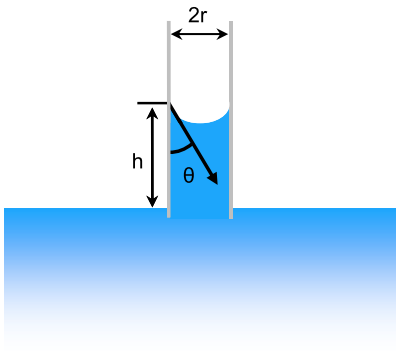


**Fig. 1.9** Illustration of a capillary tube immersed in a liquid

The above mentioned Wilhelmy balance method is probably the most reliable technique for measuring contact angles on individual fibers of known diameter. The precise value of the fiber diameter can be determined by using a liquid of known surface tension to wet the fiber completely (i.e., zero contact angle). Given that $\cos\theta = 1$, the perimeter $p$ of the fiber can be calculated from (1.4). Similar to the solid plate used in Wilhelmy balance method, a continuous immersion circle of the fiber in the liquid can also be used to test the homogeneity of the fiber surface.

### *1.3.7 Capillary Tube*

In circumstances when both the inside and outside surfaces of the capillary tube are made of the exact same material, the Wilhelmy balance method can be used to measure the contact angle. The perimeter $p$ of the capillary tube should be the sum of the inner and outer perimeters. In general, the Wilhelmy balance method can be applied to a wide range of plates, rods, wires, tubes, and capillaries.

For a vertical capillary with a sufficiently narrow circular cross section, the meniscus might be considered as spherical, and the capillary rise, $h$, is given by (Fig. 1.9):

$$h = \frac{2\gamma_{lv}\cos\theta}{\Delta\rho g r} \tag{1.6}$$

where $r$ is the capillary radius, $g$ is the acceleration constant of gravity, and $\Delta\rho$ is the difference in density between the liquid and vapor. The contact angle can be calculated using the values of experimentally measured $h$ and $r$. If $r$ is too small, it can be calculated from the length of the capillary occupied by a known mass of mercury. This relationship between contact angle, capillary height, and radius is known as the Jurin rule, named after James Jurin, who studied this effect in 1718. For relatively wide and transparent tubes, the above-mentioned Langmuir-Schaeffer reflection technique might also be used to directly measure the contact angle [83].

### 1.3.8 Capillary Penetration Method for Powders and Granules

The wetting behavior of powders and granules also involves contact angle phenomena, but it is complicated by the presence of a porous architecture. Although alternative methods have been employed to characterize porous architectures, contact angle remains the primary tool.

Direct measurement of contact angles on an individual powder or granule is almost impossible by conventional methods. Instead, the powders or granules are compressed into a flat cake, to which liquid drops are applied, and contact angles are measured [84–89]. However, due to the inherent porous architecture of compressed powder cakes, "spontaneous" liquid penetration might occur if the actual contact angle between the liquid and the solid is lower than 90°. Moreover, the actual rate of penetration might vary largely depending on the actual wettability and the porous structure. It might occur slowly enough that reproducible results can be obtained through direct measurement; or it might happen rapidly and give unstable results. Microscopic examination shows that the surfaces of compressed powders are porous, and it has been demonstrated thermodynamically that the contact angle on a porous surface is higher than on a smooth surface with the same composition [90]. The data can also be influenced by surface roughness [91, 92], particle swelling [55], and tablet porosity [61, 93]. Furthermore, during sample preparation, the topmost powder particles are likely to undergo plastic deformation by the compression, which might give different results than the uncompressed powders [61]. In addition, if the powder is slightly soluble in the measuring liquid, drops of solution saturated with the powder are used instead of the pure liquid [94].

The capillary penetration method was developed by Washburn [95], who monitored the rate at which a liquid penetrates into a compressed powder cake. The measurement was achieved by recording the depth of the liquid front intrusion as a function of time. The contact angle can then be deduced according to Washburn theory:

$$l^2 = \frac{rt\gamma_{lv}\cos\theta}{2\eta} \tag{1.7}$$

where $l$ is the depth of liquid intrusion, $\gamma_{lv}$ is the liquid surface tension, $\theta$ is the contact angle, $\eta$ is the liquid viscosity, $t$ is the time required for penetration, and $r$ represents the pore radius. Numerous qualitative measurements have been performed, and the method has been developed theoretically [96–98].

Static measurements were originally proposed by Bartell and co-workers [99–101], whose theory has been significantly extended by White [102]. The wetting liquid penetrates upward vertically through a compressed powder cake, until it reaches a height at which the capillary pressure balances the weight of the liquid in the column. This method involves measuring the pressure necessary to balance the Laplace pressure, which drives liquid into a capillary bed:

$$\Delta P = \frac{2\gamma_{lv}\cos\theta}{r} \tag{1.8}$$

where $\Delta P$ is the pressure difference, $\gamma_{lv}$ is the liquid surface tension, $\theta$ is the contact angle, and $r$ is the pore radius.

Both Washburn's and Bartell's methods suffer from the common drawback that the effective pore radius $r$ is not constant from point to point in the powder bed. White [102] defined the effective capillary radius $r_{eff}$ in the following way:

$$r_{eff} = \frac{2(1-\phi)}{\phi \rho A} \tag{1.9}$$

where $\phi$ is the volume fraction of solid in the packed bed, $\rho$ is the density of the solid material, and $A$ is the specific surface area per gram of solid. Combining (1.8) and (1.9) yields the Laplace-White equation, which is a strict thermodynamic expression for $\Delta P$ in porous media:

$$\Delta P = \frac{\gamma_{lv} \cos\theta \phi A \rho}{1-\phi} \tag{1.10}$$

For clean and chemically treated smooth glass beads, a broad agreement between White's theory and experimental data has been obtained [103]. However, it can be rather problematic to determine $r_{eff}$ directly due to the uncertainty in measuring the specific wetted area of the particles.

Diggins and co-workers [104, 105] used a second liquid that fully wet the powder, and compared its wetting behavior with the liquid of interest. Cyclohexane, with a low surface tension of 25.5 mN/m, is the most commonly used reference liquid. Prestidge and Ralston [106] reported that the success of the method relies on the correct choice of the reference liquid.

Kwok and Neumann [107] stated that, although the contact angles obtained on powder surfaces are usually not identical to Young's contact angles, the actual measured angles, along with the surface tension of the specific contacting liquid, determine the Laplace pressure $\Delta P$, which indicates the capillary penetration. In other words, it is the actual contact angle that determines the wetting behavior of this system.

Alternatively, the so-called $h$–$\epsilon$ method proposed by Kossen and Heertjes [108, 109] can be used to obtain contact angles on compressed powders. This method is based on the assumption that the powder consists of identical spheres. After the powder is compressed into a cake, it is saturated with the probe liquid, and a drop is placed on the surface. The contact angle is calculated from the height of the drop, the cake porosity, and the density and surface tension of the liquid.

Subrahmanyam and co-workers [110] compared the contact angles of quartz by the capillary penetration method and the captive bubble method. These studies found that the capillary penetration method gave results that showed a better correlation with floatability than the captive bubble method.

### *1.3.9 Capillary Bridge Method*

Restagno et al. [111, 112] developed a high-precision contact angle measuring technique, which they referred to as the "capillary bridge method". In their experiment,

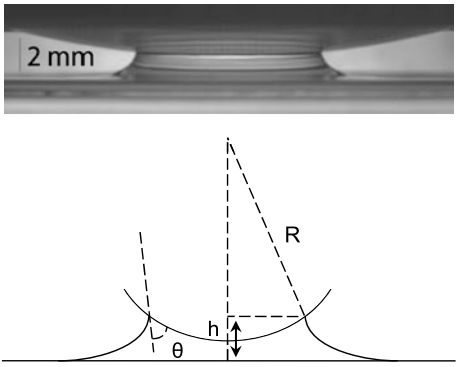


**Fig. 1.10** Photograph of a "capillary bridge", illustration of contact angle calculation. Reproduced from Ref. [111]. Copyright 2009 American Chemical Society

a spherical solid surface (usually a watch glass) is put in contact with a large liquid bath. Due to the capillary effect, a meniscus or "capillary bridge" forms around the contact line, which defines the wetted area on the solid surface. The shape of this "capillary bridge" between the solid surface and the liquid changes as the solid is slowly moved up or down to give a systematically varying wetted area. By monitoring the changes of the wetted area and the distance that solid surface moves, the dynamic contact angles can be quantitatively determined through numerical resolution of the Young-Laplace equation or by a simplified approximated relation (Fig. 1.10):

$$A = 2\pi R\left(k^{-1}\sqrt{2(1+\cos\theta)} - h\right) \tag{1.11}$$

where $A$ represents the wetted area, $h$ is the distance of solid surface from liquid bath surface, $R$ is the radius of the sphere surface, and $k^{-1}$ is the capillary length, which is known for a given liquid. The contact angle $\theta$ can be deduced from the experimentally determined $A(h)$ curve.

The capillary bridge method offers several advantages. Both advancing and receding contact angles can be established by slowly pulling the surface away from the liquid or pushing back toward the liquid; thus, the dynamic contact angles can be studied. Due to its high sensitivity, the technique can be used to characterize surfaces with low contact angle hysteresis (on the order of 1°). The technique has shown great potential in discriminating low friction surface coatings [113]. However, evaporation of the test liquid can cause uncertainty of the measured distance $h$, which will induce a small deviation in the experimental $A(h)$ curve [111]. Moreover, to measure the wetted area, the method requires transparent films to be coated on a transparent spherical surface, which can cause serious limitation and inconvenience in sample preparing [114]. This problem might be solved by introducing a new and better means to measure the wetted area.

## 1.4 Applications of the Technique

One of the most important applications of contact angle measurement is the determination of solid surface tension. The assessment of solid surface tension has been

of much fundamental and practical interest for decades [115–120]. However, solid surface tension cannot be directly measured since most existing techniques for surface tension measurement rely on surface deformation, which is difficult in the case of a solid. Several indirect methods have been developed for the assessment of solid surface tension [121], among which contact angle measurement is considered to be the simplest.

Young's equation (1.1) reveals the correlation between contact angle and interfacial tensions. It suggests that the observation of the equilibrium contact angle of liquid on solid might be a starting point for investigating the solid surface tension. However, there are only two measurable quantities in Young's equation: the contact angle $\theta$ and the liquid surface tension $\gamma_{lv}$. To determine $\gamma_{sv}$ and $\gamma_{sl}$, an additional relation between these quantities must be established.

The pioneering work of interpreting contact angles in terms of solid surface tension was carried out by Zisman and co-workers [122], who conducted numerous studies about contact angles of high-energy liquids on low-energy solid surfaces. They found out that for a given solid, the measured contact angles do not vary randomly upon change of the testing liquid. Instead, the change of $\cos\theta$ versus liquid surface tension $\gamma_{lv}$ falls into a linear trend for a homologous series of liquids such as alkanes on Teflon. In addition, extrapolation of the linear curve to where $\cos\theta = 1$ gives an important parameter, the critical surface tension $\gamma_c$. Theoretically, a liquid with a surface tension equal or less than $\gamma_c$ would wet the solid surface completely ($\theta = 0°$).

Subsequent to Zisman's work, two main groups of thoughts have developed: the surface tension components theory and the equation of state theory. Numerous methods of determining solid surface tension have been developed following these considerations. For example, Neumann and co-workers [123] measured the contact angles of a large number of liquids on solid surfaces, from which they acquired a smooth curve by plotting $\gamma_{lv}$ versus $\gamma_{lv}\cos\theta$. The curve moves in a regular way when $\gamma_{sv}$ is changed, indicating $\gamma_{lv}\cos\theta$ is dependent on $\gamma_{lv}$ and $\gamma_{sv}$, which gives the equation of state:

$$\gamma_{lv}\cos\theta = f(\gamma_{lv}, \gamma_{sv}) \tag{1.12}$$

Combining (1.12) with Young's equation (1.1), we have:

$$\gamma_{sl} = \gamma_{sv} - f(\gamma_{lv}, \gamma_{sv}) = f'(\gamma_{lv}, \gamma_{sv}) \tag{1.13}$$

As mentioned previously in Sect. 1.2.2, many experimentally accessible contact angles are not equal to Young's contact angle, and are therefore meaningless in terms of interpreting surface tension through Young's equation. Kwok and Neumann [121] developed experimental procedures and general criteria for measuring and interpreting meaningful contact angles in terms of Young's equation (1.1). Their work emphasizes that obtaining meaningful contact angles for the determination of solid surface tension depends heavily on how contact angles are measured and whether or not widely made assumptions have been violated. The assumptions are [121] (directly from the original text):

1. All approaches rely on the validity and applicability of Young's equation for surface energetic from experimental contact angles.
2. Pure liquids are always used; surfactant solutions or mixtures of liquids should not be used, since they would introduce complications due to preferential adsorption.
3. The values of $\gamma_{lv}$, $\gamma_{sv}$, and $\gamma_{sl}$ are assumed to be constant during the experiment, e.g. there should be no physical/chemical reactions between the solid and the liquid.
4. The surface tensions of the test liquids should be higher than the anticipated solid surface tension.
5. The values of $\gamma_{sv}$ in going from liquid to liquid are also assumed to be constant, e.g. independent of the liquids used.

In summary, the solid surfaces are required to be rigid, smooth, homogeneous, and inert to the testing liquids. Advancing angles should be used instead of receding angles, so as to minimize the possible swelling and physical/chemical effects. Kwok and Neumann [121] also pointed out that many results from the literature, such as non-rigid gels [124] and non-smooth biological surfaces [125], are open to question due to violations of the assumptions.

## 1.5 Recent Developments of the Technique

### *1.5.1 Drop Shape Analysis*

Numerous methods have been developed to determine the liquid surface tension and contact angle from the shape of a sessile drop, pendant drop, or captive bubble. Ideally, the shape of a liquid drop depends on the combined effects of interfacial and gravitational forces. Surface tension tends to minimize the surface area by making the drop spherical, while gravity deforms the drop in two ways: (1) by elongating a pendant drop and/or (2) flattening a sessile drop. This balance between surface tension and external forces (such as gravity) is reflected mathematically in the Laplace equation of capillarity, which offers the possibility of determining surface tension by analyzing the drop shape.

During the early years of contact angle measurement, the $\theta/2$ method was once widely used to analyze the profile of a sessile drop. In this analysis, the liquid drop is assumed to be part of a sphere. Geometrically, the contact angle can be calculated by measuring the drop diameter and the height of the apex (Fig. 1.11):

$$\frac{\theta}{2} = \tan^{-1}\left(\frac{h}{d}\right) \tag{1.14}$$

This method yields reasonable results when the liquid drop is extremely small. However, the spherical shape assumption cannot be applied if the drop shape is large enough to be affected by gravity.

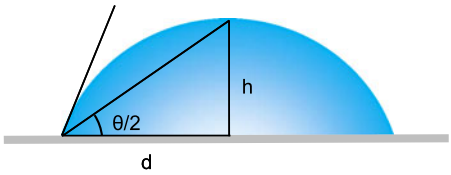


**Fig. 1.11** Demonstration of the $\theta/2$ method according to (1.14)

Bashforth and Adams [126] were the first to use the Laplace equation to analyze the shape of droplet profiles. They manually generated a collection of sessile drop profiles according to different values of surface tension and the radius of curvature at the drop apex. Consequently, the task of determining surface tension became simple interpolation from their tables. Their tremendous contribution led to booming development in the area. Blaisdell [127], as well as Tawde and Parvatikar [128] extended the Bashforth and Adams tables. Fordham [129] and Mills [130] generated equivalent tables for pendant drops. Ever since digital computers became popular, drop shape analysis has been greatly improved, and many new methods have been developed [131–141].

### *1.5.2 Axisymmetric Drop Shape Analysis (ADSA)*

During the past three decades, significant improvements were made in hardware design and computational technology, which has led to considerable development of drop shape analysis for surface science. The axisymmetric drop shape analysis (ADSA) method that was developed by Rotenberg et al. [142], improved by Spelt et al. [143], Cheng at al. [144], Río [145], and Kalantarian et al. [146] is believed to be one of the most accurate techniques for high precision contact angle measurement. With a reproducibility of $\pm 0.2°$, the ADSA method has been shown to improve the accuracy of contact angle measurement by essentially an order of magnitude, compared to the reproducibility of $\pm 2°$ by direct tangent measurements.

The basic principle of the ADSA method is to find the best theoretical profile that matches the drop profile extracted from an experimental image, from which the surface tension, contact angle, drop volume, and surface area can be computed. There are two main assumptions in the ADSA method: (1) the experimental drop is Laplacian and axisymmetric, and (2) gravity is the only external force. Surface tension is used as an adjustable parameter, and the algorithm searches for the specific value of surface tension that produces the best theoretical profile that fits the experimental drop profile. The first generation of the axisymmetric drop shape analysis-profile (ADSA-P) method was developed by Rotenberg et al. [142]. In this method, an objective function is defined as the sum of the squares of the normal distances between experimental profile points and corresponding theoretical profile points. The matching is achieved by minimizing the objective. It should be noted that extracting drop interface coordinates was performed manually in the first generation

ADSA. Cheng et al. [144] improved the first generation ADSA-P method by implementing a computer-based edge operator, Sobel [147], to extract the drop interface profiles automatically. Optical distortion correction techniques were also incorporated into the ADSA-P program to achieve better accuracy. The first generation ADSA-P method was found to give accurate results except for large and flat sessile drops, where the program failed due to the flatness of the apex.

Rio and Neumann [145] developed the second-generation ADSA-P method by integrating more efficient algorithms. They also used the curvature at the apex instead of the radius of curvature at the apex as a parameter, so as to overcome the apex limitation in the first generation ADSA-P. The vertical location of the solid surface was determined to pixel resolution from the digitized drop image.

Another branch of the ADSA method—the axisymmetric drop shape analysis-diameter (ADSA-D)—was developed to measure extremely low contact angles (less than 20°) or contact angles on non-ideal surfaces [148, 149]. Quite different from the ADSA-P method, the ADSA-D program analyzes a top view image of the drop and measures the contact diameter. Once the contact diameter, liquid surface tension, and volume of the drop are known, the contact angle can be determined from numerical integration of the Laplace equation of capillarity. It has been claimed that the contact angle results obtained by the ADSA-D and ADSA-P methods closely agree, varying no more than $\pm 0.4°$, for which ADSA-D gives a higher precision for low contact angles [148, 149]. However, Rodriguez-Valverde and co-workers [150] reported that quantification of the effects of surface roughness in contact angle measurements is unwieldy and controversial. They asserted that the equilibrium contact angle cannot be measured due to the existence of metastable states and a strong dependence on drop size.

A new drop shape analysis method called theoretical image fitting analysis (TIFA) was introduced by Cabezas et al. [151, 152]. The main difference between TIFA and ADSA is that TIFA fits the whole two-dimensional theoretical projection to the experimental image, instead of ADSA fitting only a one-dimensional theoretical profile curve to the experimental image. TIFA operates without using edge detection algorithms. Further, it employs an error function that measures pixel-by-pixel differences between the theoretical and experimental images, which are then minimized so as to fit theoretical image to the experimental image.

Both ADSA and TIFA suffer from a common limitation: the necessity of using the apex of the drop as part of the drop image analysis. For this reason, the most widely used system of a liquid drop with the needle immersed at the apex cannot be applied. Instead, drops must be formed from below the solid surface through a hole. This complication has led to the development of new versions of both methods: the TIFA-AI (theoretical image fitting analysis for axisymmetric interfaces) method [153] developed by Cabezas et al., and the ADSA-NA (axisymmetric drop shape analysis-no apex) method developed by Kalantarian et al. [146]. With TIFA-AI, the geometry of the interface at a reference level different from the apex is used to solve the Laplace equation. The radius of the profile and its inclination at the reference level are defined as two additional optimization parameters. ADSA-NA

is also able to analyze the shape of axisymmetric interfaces without using apex coordinates. A recent study shows that the contact angle data obtained using these two new methods agree within ±0.1° [146].

### *1.5.3 Contact Angle Measurement of Ultrasmall Droplets*

Wetting phenomena have been extensively investigated and well understood at the macroscale (millimeters); while the wetting behavior at the micro- or nanoscale (micro- or nanometers) has yet to be thoroughly studied, and many issues remain unresolved. The study of ultrasmall droplets on solid surfaces allows wetting theories to be tested down to the nanoscale, where the wetting behavior is significantly influenced by line tension and liquid evaporation (both are usually negligible in macroscale studies). These studies have relevance to many industrial applications, such as friction in microelectromechanical systems (MEMS) devices [154], flotation in mineral recovery [155], and wastewater treatment [156].

At the micro- or nanoscale, it is possible to take advantage of the fact that the influence of gravity is negligible compared to the influence of surface tension; consequently, the droplet can be approximated as part of a sphere [157]. There are, however, complications due to the small size. As the drop becomes smaller, the effect of the line tension at the three-phase contact line becomes larger compared to the effect of surface tension [158, 159]. For micro- or even nanometer-sized droplets, the line tension can significantly affect the measured contact angle [160]. Thus, at micro- and nanoscales, the classical Young's equation must be modified, which is usually done by adding a second term to take the line tension effect into account [159–161]:

$$\cos\theta_\infty = \frac{\gamma_{sv} - \gamma_{sl}}{\gamma_{lv}} \tag{1.15}$$

$$\cos\theta_R = \cos\theta_\infty - \frac{\sigma\gamma_{lv}}{R} \tag{1.16}$$

In these equations, $\theta$ is the contact angle, and the subscripts, $R$ and $\infty$ indicate the radius of the droplet. The quantity $\gamma$ is the surface tension, $\sigma$ is the line tension of the three-phase system, and $R$ is the radius of the drop at the surface. The subscripts $s$, $l$, and $v$ indicate the solid, liquid, and vapor phases, respectively.

Another problem associated with small droplets is the effect of evaporation, which is especially problematic when working with atomic force microscopy (AFM), because AFM requires at least 15–30 min to produce a stable image. Picknett and Bexon [162] studied the changes of droplet profile during evaporation. They found that there exist two stages: a first "constant contact area" phase dominates until the contact angle decreases to certain value, at which point a second "constant contact angle" phase dominates thereafter. This model has been supported by Soolaman and Yu [163], who reported that the evaporation of water microdroplets progresses from the pinning stage (decreasing contact angle, constant contact area)

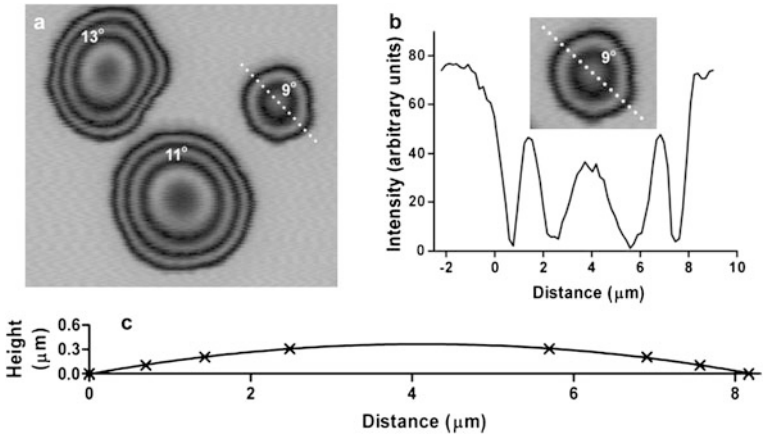


**Fig. 1.12** Interference method for measuring microscale contact angles. (**a**) Interference fringes in water droplets on ethanol-cleaned glass (image size 129 × 115 $\mu m^2$); the contact angles indicated for the droplets. (**b**) Intensity profile along the *dotted line* in (**a**) and *inset* that shows a magnification of the droplet analyzed (image size 44 × 38 $\mu m^2$). (**c**) Drop profile with circular curve fitted to the data from the *dashed line* in (**a**). Reproduced from Ref. [174]. Copyright 2007 Elsevier Science

to the shrinking stage (constant contact angle, decreasing contact area). Therefore, the evaporation effect must be taken into consideration when interpreting micro- and nanodroplets profiles.

Several methods for measuring the contact angles of ultrasmall droplets have been reported thanks to the availability of advanced imaging techniques such as interference microscopy, confocal microscopy, environmental scanning electron microscopy (ESEM), and AFM to establish the droplet profiles [164–171]. Interference microscopy method utilizes the fringe patterns formed by the interfering beams reflected from the solid-liquid and the liquid-vapor interfaces to calculate the contact angle value. It is best suited for droplets with low contact angles (less than 30°), in which case individual interference fringes are readily resolved. Jameson and Del Cerro [172] used this technique for cases in which the underlying phase is transparent. Fischer and Ovryn [173] improved the technique by developing a geometrical-optics-based model to interpret the optical path length through a thick refractive specimen.

Confocal microscopy, on the other hand, is best suited for droplets with higher contact angles (30–90°) since such droplets have greater heights, thus allowing the collection of a larger number of image slices from which the drop profile can be reconstructed. Sundberg et al. [174] recently used a combination of interference microscopy and confocal fluorescence microscopy to study the contact angles of micrometer-sized nucleated water droplets (Fig. 1.12). The method was designed for measuring both low (< 30°) and high (30–90°) contact angles. For droplets displaying low contact angles, the profiles can be reconstructed from the interference patterns, whereas for contact angles too high to allow resolution of interference fringes, a low concentration of fluorescent dye was mixed with water to allow the

recording and analysis of 3D image stacks. The results were compared with contact angles of macroscopic (millimeter scale) droplets, and a dependence of contact angle on droplet sizes was found. At small radii (below 10 μm), the contact angles obtained are larger than the macroscopic contact angles, indicating a positive line tension effect. When the radii of the droplets are more than 10 μm, the average contact angles on microscopic droplets are largely the same as their macroscopic counterparts. In general, interference and confocal methods can measure droplets with diameters of about 10 to 100 μm. New techniques with higher resolution are needed for nanoscale measurements.

A number of methods have been developed to deposit micro- and nanoscale liquid droplets on surfaces. The simplest way is to use an air sprayer [175], which generates ultrasmall droplets by mixing macroscale droplets with a jet of compressed air. Commercially available atomizers are able to spray ultrafine droplets with a wide range of sizes. Hong et al. [176] used micropipettes with submicron orifices to create submicron-sized droplets. Jayasinghe and Edirisinghe [177] used electrospraying to generate charged liquid droplets with diameters less than 1 μm. Similar methods have also been used by Paine et al. [178] and by Adhikari and Fernando [179]. Fine-emulsions and nano-emulsions formed by two immiscible phases can generate significantly smaller droplets (between 100 and 1000 nm) [180]. Zhang and Ducker [181] successfully observed ultrasmall interfacial oil nanodroplets of decane (height 2–50 nm) formed at the solid/liquid interface by direct adsorption from an emulsion. A syringe pump has also been used to create microdroplets [182]. However, with all of the aforementioned methods, control over the size of the droplet presents a challenging problem.

To address this problem, Meister et al. developed a nanoscale dispensing (NADIS) technique by modifying a commercially available silicon nitride ($Si_3N_4$) AFM probe tip and using it to transfer liquid from the tip to the surface by direct contact [183, 184]. Here, the size of the deposited droplet is controlled by the aperture width of the hollow AFM tip. The NADIS technique is able to create droplets with controlled sizes to measure the contact angle at micro- or nanoscales [185]. Jung and Bhushan [186] have used the NADIS technique to deposit micro- and nanodroplets of a glycerol/water mixture on different surfaces, followed by measuring the contact diameter, thickness, and volume of the droplet with an AFM to determine the contact angles. Fang et al. [187] have shown that tips with an aperture diameter of 35 nm were able to deposit nanodroplets of glycerol-based liquids with diameters down to 70 nm and to form regular arrays on silica surfaces with different hydrophilicities. Importantly, fine control of the droplet volume is also possible.

As mentioned previously, the capillary penetration technique based on Washburn's theory is the most frequently used technique for determining contact angle of particles. However, there exists an inherent limitation—it only gives an averaged contact angle value and thus cannot describe the wetting behavior of individual powders. In recent years, AFM has been used to study the contact angle of individual particles by measuring the interaction forces between a spherical colloidal particle and a bubble in aqueous solution [188–192]. The contact region of the AFM force

curve is used to establish the position of zero force, which gives the depth of the particle penetration into the bubble. The data can then be used to calculate the contact angle. In this way, the intrinsic hydrophobic properties of an individual particle can be revealed. It is also worth mentioning that soft surfaces can sometimes deform during AFM force measurements [193–195]. Furthermore, Nguyen and co-workers [196] observed that the contact angle measured by AFM changes with the speed of the piezoelectric translator, showing that the measurements were generally dynamic. However, it cannot be decided whether or not the measured contact angle on a single particle indicates the hydrophobicity of the solid particle surface, since the position of the three-phase contact area relative to the particle is unknown. In the case of pinning of the three-phase contact, the determined contact angle does not entirely characterize the hydrophobic properties of the particle surface. Notably, work by Jung and Bhushan [186] using the AFM-based NADIS technique to measure the contact diameter, thickness, and droplet volume gave contact angle values that were lower than those of corresponding macrodroplets.

Checco et al. [197] measured the contact angles of micro- and nanoscale alkane droplets on a model substrate using non-contact AFM. They connected an enclosed chamber to the AFM head in order to mitigate evaporation. The large range of droplet sizes accessible allowed them to determine the contact line curvature dependence of the contact angles. The contact angle values were found to decrease when the droplet size decreased from macroscopic scales. Furthermore, they found that the modified Young's equation fails to describe correctly the experimental data at a sufficiently large range of droplet sizes, and used surface heterogeneity to explain this shortcoming, which was further supported by numerical simulations. More recently, Checco et al. produced a nanoscale wettability pattern on a surface consisting of hydrophilic COOH-terminated and hydrophobic $CH_3$-terminated lines (Fig. 1.13) [198]. The use of an evaporation-condensation chamber allows control of both the temperature and the vapor concentration. By measuring the contact angle of ethanol nano-channels formed on the surface, they found that ethanol selectively wetted the hydrophilic lines with an apparent contact angle at the stripe's boundary of $12° \pm 1°$, a value significantly lower than that measured macroscopically for an ethanol droplet on the same surface ($30° \pm 1°$).

Dupres et al. also used AFM to study the local wetting of human hair [199]. For nonvolatile liquids, small droplets were directly deposited on the solid by using a microsyringe; volatile liquids were deposited in a condensation chamber. Most of the liquids tested have a higher surface tension $\gamma_{lv}$ than the critical surface tension $\gamma_c$; consequently, partial wetting is expected. However no spreading or drop nucleation was observed. Interestingly, more polar liquids such as water and glycerol failed to wet any region of the cuticle, although water seemed to penetrate into the bulk of the hair fiber. Hydrocarbon liquids preferentially wetted the more polar cuticle edges. In a more recent report, Dupres and co-workers studied the changes in wettability of the cuticle when different covalently and non-covalently bound fatty acids present at the cuticle surface were selectively extracted [200].

Wang and co-workers [201, 202] used AFM to image sprayed water microdroplets on polished metal surfaces. They found large differences between

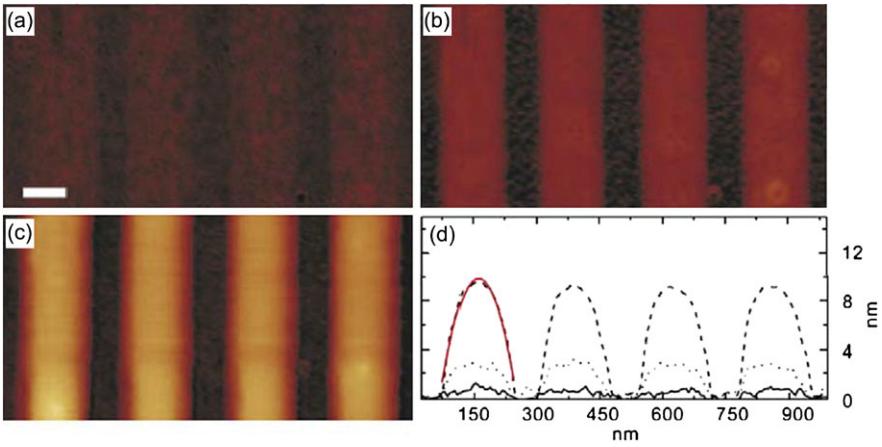


**Fig. 1.13** Condensation of ethanol onto COOH nanostripes for $\Delta$T equal to: (**a**) 10 °C, (**b**) 0.5 °C, and (**c**) −15 °C (lateral scale 100 nm). (**d**) Cross-sectional profiles corresponding to (**a**) (*solid line*), (**b**) (*dotted line*), and (**c**) (*dashed line*). Reproduced from Ref. [198]. Copyright 2006 Elsevier Science

macroscale and microscale wettability, even on the same surface. While the contact angles of macroscale water droplets were found to be larger than those of microscale water droplets, the scatter in the values of the microscale contact angles was larger than those of the macroscale contact angles. Accordingly, the shapes of the droplets could not be maintained when the droplets become too small. The influence of organic contaminants might contribute to this phenomenon. Organic contaminants in general increase surface hydrophobicity, and their distribution might be non-uniform at the micro- and nanoscale. When droplets are obtained by condensation, there should be areas with little or no organic contamination, where water preferentially condensed, leading to reduced nanoscale contact angles. This rationalization is consistent with the previously mentioned results by Checco et al. [197], who also suggested the possibility that small surface heterogeneities were responsible for the observed decrease in contact angle when the droplet size was decreased from 2 mm to 200 nm. ESEM has also been used as an imaging tool in the studies of microwetting. Stelmashenko et al. [203] performed fundamental studies on the imaging of water droplets nucleated onto different standard surfaces. Lau et al. [204] used ESEM to verify their creation of a stable, superhydrophobic surface using the nanoscale roughness inherent in a vertically aligned carbon nanotube forest together with a thin, conformal hydrophobic poly(tetrafluoroethylene) (PTFE) coating on the surface of the nanotubes. Spherical water microdroplets formed by condensing vapor onto the surface can be suspended on top of the nanotube forest. The results confirmed that the superhydrophobic characteristic is retained at the microscale. In a related superhydrophobicity study, Cheng and Rodak [205] reported that lotus leaves lost their superhydrophobic character (“lotus effect”) when microscale water droplets were condensed on the leaf.

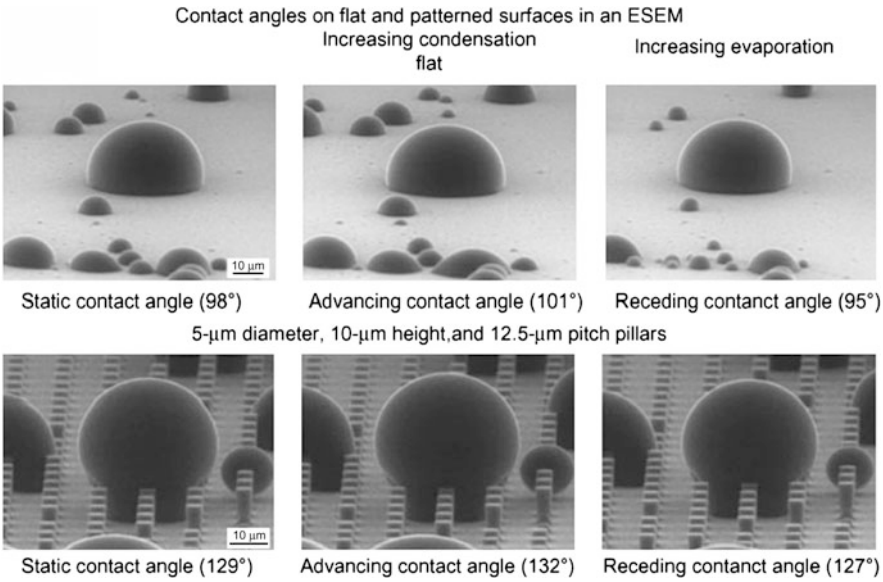


**Fig. 1.14** ESEM images of static, advancing, and receding contact angles of microscopic droplets of water on flat and patterned Si surfaces. Reproduced from Ref. [206]. Copyright 2008 The Royal Microscopical Society

Recently, Jung and Bhushan [206] reported an ESEM study of the dynamic wetting of superhydrophobic surfaces. Static contact angles were measured once a dynamic equilibrium between condensation and evaporation was achieved. Advancing contact angles were obtained by cooling the substrate so as to increase the condensation and grow the drop size. Conversely, receding angles were achieved by heating the substrate. Thus, the hysteresis was measured, which showed no obvious difference compared to macroscopic droplets. The researchers found, however, that the hysteresis depended on the geometric characteristics of the patterned surface (Fig. 1.14).

ESEM has specific advantages for characterizing micro- and nanofibers, as fibers have two dimensions at the micro/nanoscale and one dimension at the macroscale. Conventionally, the Wilhelmy balance technique was used to evaluate the wetting properties of fibers. A major limitation of this technique lies in the difficulty of precise measurement of the fiber perimeters, especially in the case of micro- and nanofibers. The use of ESEM can provide additional information at the sub-single-fiber level (Fig. 1.15) [207, 209].

Wettability studies at the micro- and nanoscale have paved the way for the development of wetting patterns. For example, it is possible to deposit droplets onto surfaces to which a chemical or topographical micro- or nanoscale pattern is imposed [208–216]. Wetting patterns, especially those obtained by patterning organic molecules, are currently of great interest in the area of molecular-scale devices [217, 218]. Figure 1.16 shows work done by Seemann et al. [216], who created

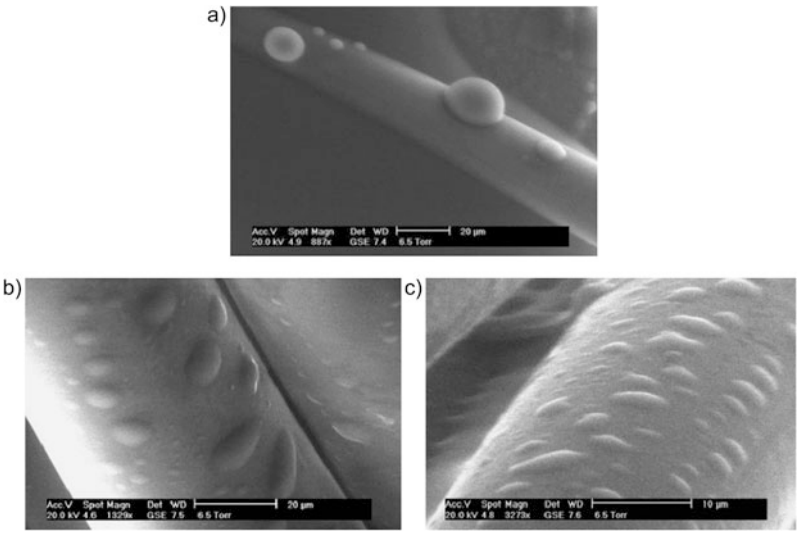


**Fig. 1.15** ESEM images of water microdroplets on polypropylene (PP) fibers: (**a**) untreated; (**b**) oxygen-plasma treated for 30 s; (**c**) oxygen-plasma treated for 60 s. Reproduced from Ref. [209]. Copyright 2004 Elsevier Science

grooves with rectangular cross sections in Si by photolithographic methods with depths between 100 and 900 nm, and widths between 400 nm and 3 mm. These studies introduced a global morphology diagram of clustering droplet geometries that depends on the aspect ratio of the groove geometry and the contact angle of the substrate. To sum up, these studies on wetting patterns have revealed the occurrence of morphological wetting and dewetting transitions, which has promising applications in electrowetting, microfluidics, and nanodevice development.

## 1.6 Summary

In this report, the basic and advanced techniques used to characterize the wettability of materials at the macro-, micro-, and nanoscale have been described. As the importance of wettability in both fundamental and applied fields has long been recognized, innovative techniques for measuring the wettability of surfaces, powders, and fibers continue to emerge. Nevertheless, there are still many open questions regarding wetting mechanisms and for manipulating the wetting behavior at the micro- and nanoscales. AFM and ESEM are currently the most relevant techniques for imaging ultrasmall droplets on surfaces. AFM provides high resolution at the nanometer scale, but is limited by long measurement times. For example, measurements by AFM routinely require 15–30 min to acquire a stable image, which can be a great disadvantage because some nanodroplets evaporate in seconds. ESEM, on the other hand, collects images rapidly (in seconds), which circumvents evaporative

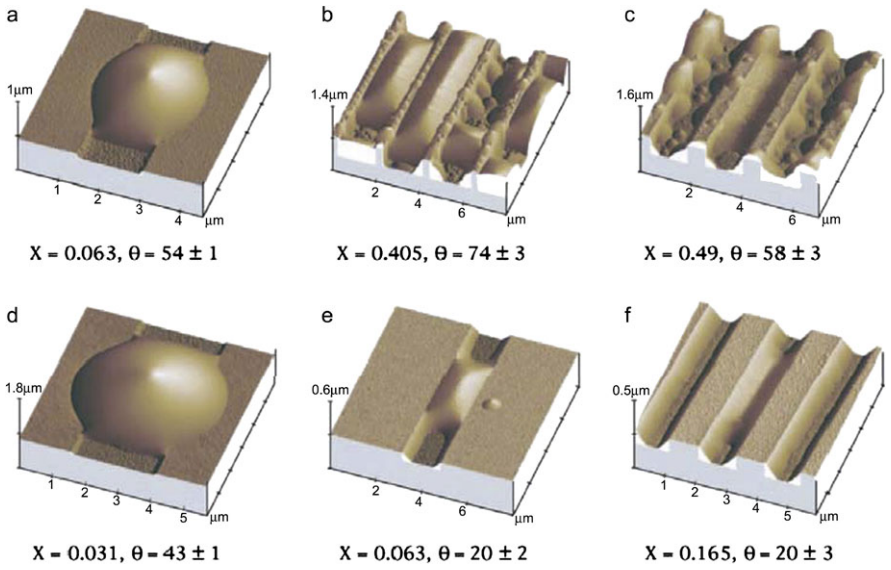


**Fig. 1.16** AFM images of liquid structures in grooves with rectangular cross section. Reproduced from Ref. [216]. Copyright 2005 National Academy of Science, USA

problems and allows the collection of dynamic contact angles. However, the resolution of ESEM is only at the micrometer scale. The use of a field emission gun (FEG) in ESEM is expected to diminish beam effects and enhance the resolution to the nanometer range. As for AFM, there are current developments in both the electronic and the data acquisition systems, as well as in the design of AFM probes optimized for high-speed scanning (especially small cantilevers) [219]. Hopefully, we will witness these significant advances applied to future wettability studies and practices.

**Acknowledgements** We acknowledge generous financial support from the National Science Foundation (DMR-0906727), the Robert A. Welch Foundation (Grant No. E-1320), and the Texas Center for Superconductivity at the University of Houston.

## References

1. K.N. Prabhu, P. Fernandes, G. Kumar, Mater. Des. **2**, 297 (2009)
2. X. Zhao, M.J. Blunta, J.J. Yao, Pet. Sci. Technol. Eng. **71**, 169 (2010)
3. Y.Q. Wang, H.F. Yang, Q.G. Hang, L. Fang, S.R. Ge, Adv. Mater. Res. **154–155**, 1019 (2010)
4. M. Sakai, T. Yanagisawa, A. Nakajima, Y. Kameshima, K. Okada, Langmuir **25**, 13 (2009)
5. Y. Son, C. Kim, D.H. Yang, D.J. Ahn, Langmuir **24**, 2900 (2008)
6. J. Perelaer, C.E. Hendriks, A.W.M. de Laat, U.S. Schubert, Nanotechnology **20**, 165303 (2009)
7. H. Yang, P. Jiang, Langmuir **26**, 12598 (2010)
8. B. Bhushan, Y.C. Jung, K. Koch, Langmuir **25**, 3240 (2009)

9. M. Rauscher, S. Dietrich, Annu. Rev. Mater. Sci. **38**, 143 (2008)
10. K. Fei, C.P. Chiu, C.W. Hong, Microfluid. Nanofluid. **4**, 321 (2008)
11. Z. Keshavarz-Motamed, L. Kadem, A. Dolatabadi, Microfluid. Nanofluid. **8**, 47 (2010)
12. Y.S. Nanayakkara, S. Perera, S. Bindiganavale, E. Wanigasekara, H. Moon, D.W. Armstrong, Anal. Chem. **82**, 3146 (2010)
13. A. Lafuma, D. Quere, Nat. Mater. **2**, 457 (2003)
14. J.H. Snoeijer, B. Andreotti, Phys. Fluids **20**, 057101 (2008)
15. T. Young, Philos. Trans. R. Soc. Lond. **95**, 65 (1805)
16. R.E. Johnson Jr., R.H.J. Dettre, Phys. Chem. **68**, 1744 (1964)
17. L.W. Schwartz, S. Garoff, Langmuir **1**, 219 (1985)
18. J.F. Joanny, P.G.J. de Gennes, Chem. Phys. **81**, 552 (1984)
19. J.W. Krumpfer, T.J. McCarthy, Faraday Discuss. **146**, 103 (2010)
20. L. Gao, T.J. McCarthy, Langmuir **22**, 6234 (2006)
21. A.W. Neumann, Adv. Colloid Interface Sci. **4**, 105 (1974)
22. D. Li, A.W. Neumann, in *Applied Surface Thermodynamics*, ed. by J.K. Spelt, A.W. Neumann (Dekker, New York, 1996), p. 109
23. R.V. Sedev, J.G. Petrov, A.W. Neumann, J. Colloid Interface Sci. **180**, 36 (1996)
24. R.N. Wenzel, Ind. Eng. Chem. **28**, 988 (1936)
25. S. Baxer, A.B.D.J. Cassie, Tex. Inst. **36**, 67 (1945)
26. J.K. Spelt, D.R. Absolom, A.W. Neumann, Langmuir **2**, 620 (1986)
27. B.B. Davidson, G.J. Lei, Polym. Sci. **9**, 569 (1971)
28. T.R. Krishman, I. Abraham, E.I. Vargha-Butler, Int. J. Pharm. **80**, 277 (1992)
29. C.D. Bain, E.B. Troughton, Y. Tao, J. Eval, G.M. Whitesides, R.O. Nuzzo, J. Am. Chem. Soc. **111**, 321 (1989)
30. C.D. Bain, G.M. Whitesides, Angew. Chem. Int. Ed. **28**, 506 (1989)
31. E.F. Hare, E.G. Shafrin, W.A.J. Zisman, Phys. Chem. **58**, 236 (1953)
32. C.J. Budziak, E.I. Vargha-Butler, A.W.J. Neumann, Appl. Polym. Sci. **42**, 1991 (1959)
33. A. Dilks, B. Kay, Macromol. **14**, 855 (1981)
34. H.J. Yasuda, Polym. Sci. **16**, 199 (1981)
35. E.I. Vargha-Butler, M. Kashi, H.A. Hamza, A.W. Neumann, Coal Prep. **3**, 53 (1986)
36. H.J. Busseher, A.W.J. van Pelt, H.P. De Jong, J. Arends, J. Colloid Interface Sci. **95**, 23 (1983)
37. W.C. Bigelow, D.L. Pickett, W.A.J. Zisman, Coll. Sci. **1**, 513 (1946)
38. J. Leja, G.W. Poling, On the interpretation of contact angle, in *Proceedings of the 5th Mineral Processing Congress* (IMM, London, 1960), p. 325
39. R.W. Smithwich, J. Colloid Interface Sci. **123**, 482 (1988)
40. D.Y. Kwok, R. Lin, M. Mui, A.W. Neumann, Colloids Surf. A **116**, 63 (1996)
41. S. Brandon, N. Haimovich, E. Yeger, A. Marmur, J. Colloid Interface Sci. **263**, 237 (2003)
42. P. Letellier, A. Mayaffre, M. Turmine, J. Colloid Interface Sci. **314**, 604 (2007)
43. A.W. Neumann, R.J. Good, in *Surface and Colloid Science: Experimental Methods*, vol. 11, ed. by R.J. Good, R.R. Stromberg (Plenum Publishing, New York, 1979), p. 31
44. R.J. Hunter, *Foundations of Colloid Science*, 2nd edn. (Clarendon Press, Oxford, 2001)
45. G. MacDougall, C. Ockrent, Proc. R. Soc. **180A**, 151 (1942)
46. C.W. Extrand, Y. Kumagai, J. Colloid Interface Sci. **184**, 191 (1996)
47. C.W. Extrand, Y. Kumagai, J. Colloid Interface Sci. **191**, 378 (1997)
48. E. Pierce, F.J. Carmona, A. Amirfazli, Colloids Surf. A **323**, 73 (2008)
49. B. Krasovitski, A. Marmur, Langmuir **21**, 3881 (2005)
50. W.A. Zisman, Adv. Chem. Ser. **87**, 1 (1968)
51. M.C. Phillips, A.C. Riddiford, J. Colloid Interface Sci. **41**, 77 (1972)
52. D.E. McIntyre, A study of dynamic wettability on a hydrophobic surface, Ph.D. Thesis, The Institute of Paper Chemistry, Appleton, WI, 1969
53. W.J. Fenrick, Rev. Sci. Instrum. **35**, 1616 (1964)
54. L.R. Fisher, J. Colloid Interface Sci. **72**, 200 (1979)
55. I. Langmuir, V.J. Schaeffer, J. Am. Chem. Soc. **59**, 2400 (1937)

56. T. Fort, H.T. Patterson, J. Colloid Interface Sci. **29**, 185 (1967)
57. K.A. Johnson, D.O. Shah, J. Colloid Interface Sci. **107**, 1 (1985)
58. A.F. Taggart, T.C. Taylor, C.R. Ince, Trans. Am. Inst. Min. Metall. Pet. Eng. **87**, 285 (1930)
59. W. Zhang, M. Wahlgren, B. Sivik, Desalination **72**, 263 (1989)
60. N.K. Adam, G.J. Jessop, Chem. Soc. **127**, 1863 (1925)
61. F.M. Fowkes, W.D. Harkins, J. Am. Chem. Soc. **62**, 337 (1940)
62. A.L. Spreece, C.P. Rutkowski, G.L. Gaines Jr., Rev. Sci. Instrum. **28**, 636 (1957)
63. G.T. Smedley, D.E. Coles, J. Colloid Interface Sci. **286**, 310 (2005)
64. B.A. Bezuglyi, O.A. Tarasov, A.A. Fedorets, Colloid J. **63**, 668 (2001)
65. L.A. Wilhelmy, Ann. Phys. **119**, 117 (1863)
66. H.M. Princen, J. Colloid Interface Sci. **30**, 69 (1969)
67. J.C. Cain, D.W. Francis, R.D. Venter, A.W. Neumann, J. Colloid Interface Sci. **94**, 123 (1983)
68. M. Shimokawa, T. Takamura, J. Electroanal. Chem. Interfacial Electrochem. **41**, 359 (1973)
69. A.W. Neumann, Z. Phys. Chem. **41**, 339 (1964)
70. C.J. Budziak, E.I. Vargha-Butler, A.W. Neumann, J. Appl. Polym. Sci. **42**, 1959 (1991)
71. C.J. Budziak, A.W. Neumann, Colloids Surf. **43**, 279 (1990)
72. D.Y. Kwok, C.J. Budziak, A.W. Neumann, J. Colloid Interface Sci. **173**, 143 (1995)
73. D.D. Jordan, J.E. Lane, Austral. J. Chem. **17**, 7 (1964)
74. A.W. Neumann, W. Tanner, Tenside **4**, 220 (1967)
75. J. Kloubek, A.W. Neumann, Tenside **6**, 4 (1969)
76. A.M. Schwartz, F.W. Minor, J. Colloid Sci. **14**, 572 (1959)
77. A.M. Schwartz, C.A. Rader, Congr. Surface Activity Brussels **2**, 383 (1964)
78. W.D. Bascom, J.B. Romans, Ind. Eng. Chem. Prod. Res. Dev. **7**, 172 (1968)
79. R.J. Roe, J. Colloid Interface Sci. **50**, 70 (1975)
80. H.M. Princen, in *Surface and Colloid Science*, vol. 2, ed. by E. Matijevic (Wiley, New York, 1969), p. 1
81. A.V. Rapacchietta, A.W. Neumann, S.N. Omenyi, J. Colloid Interface Sci. **59**, 541 (1977)
82. A.V. Rapacchietta, A.W. Neumann, J. Colloid Interface Sci. **59**, 555 (1977)
83. R.J. Good, J.K. Pascheck, in *Wetting, Spreading and Adhesion*, ed. by F. Paddy (Academic Press, New York, 1978), p. 147
84. G. Zografi, S.S. Tam, J. Pharm. Sci. **65**, 1145 (1976)
85. C.F. Lerk, M. Lagas, J.P. Boelstra, P. Broersma, J. Pharm. Sci. **66**, 1480 (1977)
86. W.C. Liao, J.L. Zatz, J. Pharm. Sci. **68**, 488 (1979)
87. V. Steiner, G. Adam, Cell Biophys. **6**, 279 (1984)
88. E.I. Vargha-Butler, S.J. Sveinsson, Z. Policova, Colloids Surf. **58**, 271 (1991)
89. A.W. Neumann, D. Renzow, H. Reumuth, I.E. Richter, Colloid Polym. Sci. **55**, 49 (1991)
90. R. Shuttleworth, G.L.J. Bailey, Discuss. Faraday Soc. **3**, 16 (1948)
91. G. Buckton, J.M. Newton, Powder Technol. **46**, 201 (1986)
92. D.T. Hansford, D.J.W. Grant, J.M. Newton, Powder Technol. **26**, 119 (1980)
93. G. Buckton, J.M. Newton, J. Pharm Pharmacol. **37**, 605 (1985)
94. A. Stamm, D. Gissinger, C. Boymond, Drug Dev. Ind. Pharm. **10**, 381 (1984)
95. E.W. Washburn, Phys. Rev. **17**, 374 (1921)
96. S. Levine, J. Lowndes, E.J. Watson, G. Neale, J. Colloid Interface Sci. **73**, 136 (1980)
97. R.J. Good, N.J. Lin, J. Colloid Interface Sci. **54**, 52 (1976)
98. L.R. Fisher, P.D. Lark, J. Colloid Interface Sci. **69**, 486 (1979)
99. F.E. Bartell, H.J. Osterhof, Ind. Eng. Chem. **19**, 1277 (1927)
100. F.E. Bartell, C.E. Whitney, J. Phys. Chem. **36**, 3115 (1932)
101. F.E. Bartell, C.W. Walton, J. Phys. Chem. **38**, 503 (1934)
102. L.R. White, J. Colloid Interface Sci. **90**, 536 (1982)
103. D. Dunstan, L.R. White, J. Colloid Interface Sci. **111**, 60 (1986)
104. D. Diggins, J. Ralston, Coal Prep. **13**, 1 (1993)
105. D. Diggins, L.G.J. Fokkink, J. Ralston, Colloids Surf. **44**, 299 (1990)
106. C.A. Prestidge, J. Ralston, J. Colloid Interface Sci. **172**, 302 (1995)

107. D.Y. Kwok, A.W. Neumann, in *Surface Characterization Methods: Principles, Techniques and Applications*, ed. by A.J. Milling (Marcel Dekker, New York, 1999), p. 37
108. N.W.F. Kossen, P.M. Heertjes, Chem. Eng. Sci. **20**, 593 (1965)
109. P.M. Heertjes, N.W.F. Kossen, Powder Technol. **1**, 33 (1967)
110. T.V. Subrahmanyam, M.B.M. Monte, A. Middea, E. Valdiviezo, F.F. Lins, Miner. Eng. **12**, 1347 (1999)
111. F. Restagno, C. Poulard, C. Cohen, L. Vagharchakian, L. Léger, Langmuir **25**, 11188 (2009)
112. L. Vagharchakian, F. Restagno, L. Léger, J. Phys. Chem. B **113**, 3769 (2009)
113. C. Cohen, F. Restagno, C. Poulard, L. Léger, Langmuir **26**, 15345 (2010)
114. R. Rioboo, M. Voué, H. Adão, J. Conti, A. Vaillant, D. Seveno, J. De Coninck, Langmuir **26**, 4873 (2010)
115. R.E. Johnson Jr., R.H. Dettre, in *Surface and Colloid Science*, vol. 2, ed. by E. Matijevic (Wiley-Interscience, Weinheim, 1969), p. 85
116. A.W. Neumann, in *Wetting, Spreading and Adhesion*, ed. by J.F. Padday (Academic Press, London, 1978), p. 3
117. A.W. Neumann, R.J. Good, *Surface and Colloid Science*, vol. 11, ed. by R.J. Good, R.R. Stromberg (Plenum Press, New York, 1979), p. 31
118. A. Marmur, Soft Matter **2**, 12 (2006)
119. A. Marmur, Annu. Rev. Mater. Res. **39**, 473 (2009)
120. A. Marmur, in *Contact Angle, Wettability, and Adhesion*, vol. 6, ed. by K.L. Mittal (Brill, Leiden, 2009), p. 3
121. D.Y. Kwok, A.W. Neumann, in *Contact Angle, Wettability and Adhesion*, vol. 3, ed. by K.L. Mittal (VSP International Science, Boston, 2003), p. 117
122. W.A. Zisman, in *Contact Angle, Wettability and Adhesion: Advances in Chemistry Series*, vol. 43, ed. by R.F. Gould (ACS, Washington, 1964), p. 1
123. A.W. Neumann, R.J. Good, C.J. Hope, M. Sejpal, J. Colloid Interface Sci. **49**, 291 (1974)
124. C.J. van Oss, L. Ju, M.K. Chaudhury, R.J. Good, J. Colloid Interface Sci. **128**, 313 (1989)
125. C.J. van Oss, R.J. Good, J. Macromol. Sci. A **26**, 1183 (1989)
126. F. Bashforth, J.C. Adams, *An Attempt to Test the Theory of Capillary Action* (Cambridge, London, 1892)
127. B.E. Blaisdell, J. Math. Phys. **19**, 186 (1940)
128. N.R. Tawde, K.G. Parvatikar, Indian J. Phys. **32**, 174 (1958)
129. S. Fordham, Proc. R. Soc. Lond. **194A**, 1 (1948)
130. O.S. Mills, Br. J. Appl. Phys. **4**, 24 (1953)
131. S. Hartland, R.W. Hartley, *Axisymmetric Fluid-Liquid Interfaces* (Elsevier, Amsterdam, 1976)
132. J.D. Malcolm, H.M. Paynter, J. Colloid Interface Sci. **82**, 269 (1981)
133. C. Maze, G. Burnet, Surf. Sci. **13**, 451 (1969)
134. C. Maze, G. Burnet, Surf. Sci. **24**, 335 (1971)
135. C. Huh, R.L. Reed, J. Colloid Interface Sci. **91**, 472 (1983)
136. J.F. Boyce, S. Schürch, Y. Rotenberg, A.W. Neumann, Colloids Surf. **9**, 307 (1984)
137. S.H. Anastasiadis, J.K. Chen, A.P. Koberstein, A.P. Siegel, J.E. Sohn, J.A. Emerson, J. Colloid Interface Sci. **119**, 55 (1986)
138. R.V. Hoggs, *An Introduction to Robust Estimation* (Academic Press, New York, 1979)
139. P. Cheng, Automation of axisymmetric drop shape analysis using digital image processing, Ph.D. Thesis, University of Toronto, Toronto, 1990
140. O.I. del Río, On the generalization of axisymmetric drop shape analysis, M.S. Thesis, University of Toronto, Toronto, 1993
141. L.R. Fisher, J.N. Israelachvili, J. Colloid Interface Sci. **80**, 528 (1981)
142. Y. Rotenberg, L. Boruvka, A.W. Neumann, J. Colloid Interface Sci. **93**, 169 (1983)
143. J.K. Spelt, Y. Rotenberg, D.R. Absolom, A.W. Neumann, Colloids Surf. **24**, 127 (1987)
144. P. Cheng, D. Li, L. Boruvka, Y. Rotenberg, A.W. Neumann, Colloids Surf. **43**, 151 (1990)
145. O.I. del Río, A.W. Neumann, J. Colloid Interface Sci. **196**, 136 (1997)
146. A. Kalantarian, R. David, A.W. Neumann, Langmuir **25**, 14146 (2009)

147. R.O. Duda, P.E. Hart, *Pattern Classification and Scene Analysis* (Wiley, New York, 1973)
148. F.K. Skinner, Y. Rotenberg, A.W. Neumann, J. Colloid Interface Sci. **130**, 25 (1989)
149. E. Moy, P. Cheng, Z. Policova, S. Treppo, D. Kwok, D.R. Mack, P.M. Sherman, A.W. Neumann, Colloids Surf. **58**, 215 (1991)
150. M.A. Rodríguez-Valverde, M.A. Cabrerizo-Vílchez, P. Rosales-López, A. Pàez-Dueñas, R. Hidalgo-Àlvarez, Colloids Surf. **206**, 485 (2002)
151. M.G. Cabezas, A. Bateni, J.M. Montanero, A.W. Neumann, Appl. Surf. Sci. **238**, 480 (2004)
152. M.G. Cabezas, A. Bateni, J.M. Montanero, A.W. Neumann, Colloids Surf. **255**, 193 (2005)
153. M.G. Cabezas, A. Bateni, J.M. Montanero, A.W. Neumann, Langmuir **22**, 10053 (2006)
154. B. Bhushan, *Handbook of Nanotechnology*, 2nd edn. (Springer, Heidelberg, 2007)
155. E. Abkhoshka, M. Korb, B. Rezaic, Expert Syst. Appl. **37**, 5201 (2010)
156. K.A. Matis, E.N. Peleka, Sep. Sci. Technol. **45**, 2465 (2010)
157. J. Chatterjee, J. Colloid Interface Sci. **259**, 139 (2003)
158. A. Marmur, J. Colloid Interface Sci. **186**, 462 (1997)
159. D.Q. Li, Colloids Surf. A **116**, 1 (1996)
160. R. David, A.W. Neumann, in *Applied Surface Thermodynamics*, vol. 151, ed. by A.W. Neumann, R. David, Y. Zuo (Taylor & Francis, Boca Raton, 2011), p. 701
161. B.A. Pethica, J. Colloid Interface Sci. **62**, 567 (1977)
162. H.Z. Yu, D.M. Soolaman, A.W. Rowe, J.T. Banks, Chem. Phys. Chem. **5**, 1035 (2004)
163. D.M. Soolaman, H.Z. Yu, J. Phys. Chem. B **109**, 17967 (2005)
164. J.P.S. Farinha, M.A. Winnik, K.G. Hahn, Langmuir **16**, 3391 (2000)
165. K.W. Stockelhuber, B. Radoev, H.J. Schulze, Colloids Surf. A **156**, 323 (1999)
166. A. Dussaud, M. Vignes-Adler, Langmuir **13**, 581 (1997)
167. F. Rieutord, M.J. Salmeron, Phys. Chem. B **102**, 3941 (1998)
168. L. Kao R, D.R. Wasan, A.D. Nikolov, D.A. Edwards, Colloids Surf. **34**, 389 (1989)
169. E. Grimoldi, S. Zanini, R.A. Siliprandi, C. Riccardi, Eur. Phys. J. D **54**, 165 (2009)
170. Z. Tao, B. Bhushan, J. Phys. D: Appl. Phys. **39**, 3858 (2006)
171. Y.-F. Gao, Y. Yang, D.-Y. Sun, Chin. Phys. Lett. **28**, 036102 (2011)
172. G.J. Jameson, M.C.G. Del Cerro, J. Chem. Soc. Faraday Trans. I **72**, 833 (1976)
173. D.G. Fisher, B. Ovryn, Opt. Lett. **25**, 478 (1979)
174. M. Sundberg, A. Månsson, S. Tågerud, J. Colloid Interface Sci. **313**, 454 (2007)
175. T. Pompe, S. Herminghaus, Phys. Rev. Lett. **85**, 1930 (2000)
176. M. Hong, K.H. Kim, J. Bae, W. Jhe, Appl. Phys. Lett. **77**, 2604 (2000)
177. S.N. Jayasinghe, M.J. Edirisinghe, J. Aerosol. Sci. **33**, 1379 (2002)
178. M.D. Paine, M.S. Alexander, K.L. Smith, M. Wang, J.P.W. Stark, J. Aerosol. Sci. **38**, 315 (2007)
179. S. Adhikari, S. Fernando, Trans. ASABE **49**, 1269 (2006)
180. T.G. Mason, J.N. Wilking, K. Meleson, C.B. Chang, S.M. Graves, J. Phys. Condens. Matter **18**, R635 (2006)
181. X.H. Zhang, W. Ducker, Langmuir **24**, 110 (2008)
182. Y. Tan, V. Cristini, A.P. Lee, Sens. Actuators B, Chem. **114**, 350 (2006)
183. A. Meister, S. Jeney, M. Liley, T. Akiyama, U. Staufer, N.F. de Rooij, H. Heinzelmann, Microelectron. Eng. **67–68**, 644 (2003)
184. A. Meister, M. Liley, J. Brugger, R. Pugin, H. Heinzelmann, Appl. Phys. Lett. **85**, 6260 (2004)
185. A. Meister, J. Polesel-Maris, P. Niedermann, J. Przybylska, P. Studer, M. Gabi, P. Behr, T. Zambelli, M. Liley, J. Vörös, H. Heinzelmann, Microelectron. Eng. **86**, 1481 (2009)
186. Y.C. Jung, B.J. Bhushan, Vac. Sci. Technol. A **26**, 777 (2008)
187. A. Fang, E. Dujardin, T. Ondarçuhu, Nano Lett. **6**, 2368 (2006)
188. M. Preuss, H.-J. Butt, Langmuir **14**, 3164 (1998)
189. S. Ecke, M. Preuss, H.-J. Butt, J. Adhes. Sci. Technol. **13**, 1181 (1999)
190. M. Preuss, H.-J. Butt, Int. J. Miner. Process. **56**, 99 (1999)
191. J. Ralston, D. Fornasiero, R. Hayes, Int. J. Miner. Process. **56**, 133 (1999)
192. D. Johnson, N. Hilal, K. Waters, K. Hadler, J. Cilliers, Langmuir **25**, 4880 (2009)

193. H.-J. Butt, A. Doppenschmidt, G. Huttl, E. Muller, O.I. Vinogradova, J. Chem. Phys. **113**, 1194 (2000)
194. H.K. Christenson, Langmuir **12**, 1404 (1996)
195. J.L. Parker, P.J. Attard, Phys. Chem. **96**, 398 (1992)
196. A.V. Nguyen, J. Nalaskowski, J.D. Miller, J. Colloid Interface Sci. **262**, 303 (2003)
197. A. Checco, P. Guenoun, J. Daillant, Phys. Rev. Lett. **91**, 186101 (2003)
198. A. Checco, Y. Cai, O. Gang, B.M. Ocko, Ultramicroscopy **106**, 703 (2006)
199. V. Dupres, T. Camesano, D. Langevin, A. Checco, P. Guenoun, J. Colloid Interface Sci. **269**, 329 (2004)
200. V. Dupres, D. Langevin, P. Guenoun, A. Checco, G. Luengo, F. Leroy, J. Colloid Interface Sci. **306**, 34 (2007)
201. R. Wang, L. Cong, M. Kido, Appl. Surf. Sci. **191**, 74 (2002)
202. R. Wang, M. Takeda, M. Kido, Mater. Lett. **54**, 140 (2002)
203. N.A. Stelmashenko, J.P. Craven, A.M. Donald, E.M. Terentjev, B.L. Thiel, J. Microsc. **204**, 172 (2001)
204. K.K.S. Lau, J. Bico, K.B.K. Teo, M. Chhowalla, G.A.J. Amaratunga, W.I. Milne, G.H. McKinley, K.K. Gleason, Nano Lett. **3**, 1701 (2003)
205. Y.T. Cheng, D.E. Rodak, Appl. Phys. Lett. **86**, 144101 (2005)
206. Y.C. Jung, B.J. Bhushan, Microsc. **229**, 127 (2008)
207. Q.F. Wei, R.R. Mather, A.F. Fotheringham, R.D. Yang, Tex. Res. J. **73**, 557 (2003)
208. D. Aronov, M. Molotskii, G. Rosenman, Appl. Phys. Lett. **90**, 104104 (2007)
209. Q.F. Wei, Mater. Charact. **52**, 231 (2004)
210. D. Aronov, M. Molotskii, G. Rosenman, Phys. Rev. B, Condens. Matter **76**, 035437 (2007)
211. M. Morita, T. Koga, H. Otsuka, A. Takahara, Langmuir **21**, 911 (2005)
212. J. Léopoldś, P. Damman, Nat. Mater. **5**, 957 (2006)
213. A. Checco, O. Gang, B.M. Ocko, Phys. Rev. Lett. **96**, 056104 (2006)
214. K. Khare, S. Herminghaus, J.-C. Baret, B.M. Law, M. Brinkmann, R. Seemann, Langmuir **23**, 12997 (2007)
215. K. Fukuzawa, T. Deguchi, J. Kawamura, Y. Mitsuya, T. Muramatsu, H. Zhang, Appl. Phys. Lett. **87**, 203108 (2005)
216. R. Seemann, M. Brinkmann, E.J. Kramer, F.F. Lange, R. Lipowsky, Proc. Natl. Acad. Sci. USA **102**, 1848 (2005)
217. L. Valentini, F. Mengoni, J.M. Kenny, A. Marrocchi, A. Taticchi, Small **3**, 1200 (2007)
218. C. Joachim, J.K. Gimzewski, A. Aviram, Nature **408**, 541 (2000)
219. A. Méndez-Vilas, A.B. Jódar-Reyes, M.L. González-Martín, Small **5**, 1366 (2009)

http://www.springer.com/978-3-642-34242-4

Surface Science Techniques
Bracco, G.; Holst, B. (Eds.)
2013, XXIII, 663 p., Hardcover
ISBN: 978-3-642-34242-4